SINTEF
PROCEEDINGS
2

Proceedings of the 12th International Conference on Computational Fluid Dynamics in the Oil & Gas, Metallurgical and Process Industries

Progress in Applied CFD – CFD2017

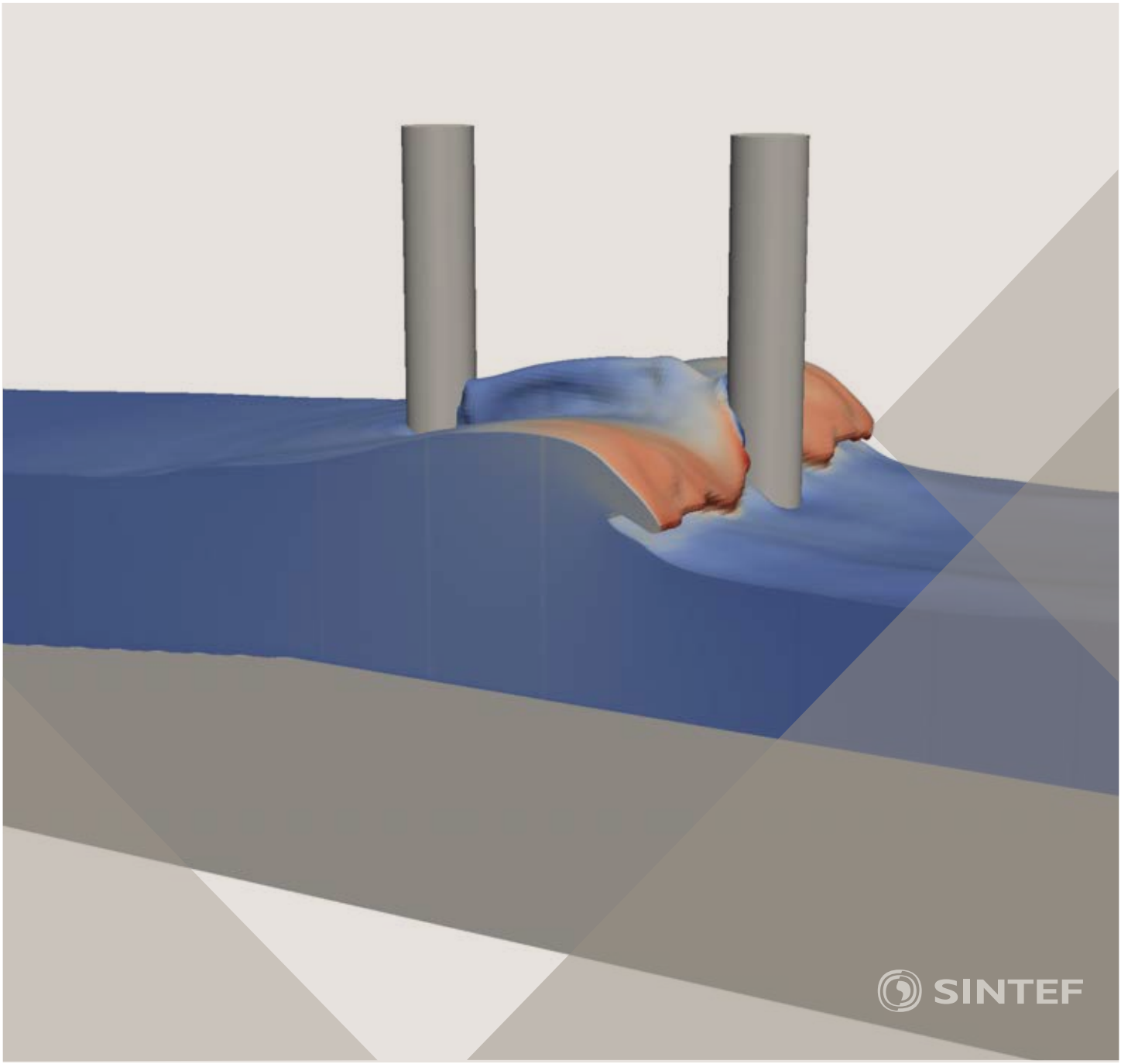

SINTEF Proceedings

Editors:
Jan Erik Olsen and Stein Tore Johansen

Progress in Applied CFD – CFD2017

Proceedings of the 12th International Conference on Computational Fluid Dynamics in the Oil & Gas, Metallurgical and Process Industries

SINTEF Academic Press

SINTEF Proceedings no 2
Editors: Jan Erik Olsen and Stein Tore Johansen
Progress in Applied CFD – CFD2017
Selected papers from 10th International Conference on Computational Fluid Dynamics in the Oil & Gas, Metallurgical and Process Industries

Key words:
CFD, Flow, Modelling

Cover, illustration: Arun Kamath

ISSN 2387-4295 (online)
ISBN 978-82-536-1544-8 (pdf)

SINTEF Academic Press
Address: Forskningsveien 3 B
PO Box 124 Blindern
N-0314 OSLO
Tel: +47 73 59 30 00
Fax: +47 22 96 55 08

www.sintef.no/byggforsk
www.sintefbok.no

SINTEF Proceedings
SINTEF Proceedings is a serial publication for peer-reviewed conference proceedings on a variety of scientific topics.
The processes of peer-reviewing of papers published in SINTEF Proceedings are administered by the conference organizers and proceedings editors. Detailed procedures will vary according to custom and practice in each scientific community.

PREFACE

This book contains all manuscripts approved by the reviewers and the organizing committee of the 12th International Conference on Computational Fluid Dynamics in the Oil & Gas, Metallurgical and Process Industries. The conference was hosted by SINTEF in Trondheim in May/June 2017 and is also known as CFD2017 for short. The conference series was initiated by CSIRO and Phil Schwarz in 1997. So far the conference has been alternating between CSIRO in Melbourne and SINTEF in Trondheim. The conferences focuses on the application of CFD in the oil and gas industries, metal production, mineral processing, power generation, chemicals and other process industries. In addition pragmatic modelling concepts and bio-mechanical applications have become an important part of the conference. The papers in this book demonstrate the current progress in applied CFD.

The conference papers undergo a review process involving two experts. Only papers accepted by the reviewers are included in the proceedings. 108 contributions were presented at the conference together with six keynote presentations. A majority of these contributions are presented by their manuscript in this collection (a few were granted to present without an accompanying manuscript).

The organizing committee would like to thank everyone who has helped with review of manuscripts, all those who helped to promote the conference and all authors who have submitted scientific contributions. We are also grateful for the support from the conference sponsors: ANSYS, SFI Metal Production and NanoSim.

Stein Tore Johansen & Jan Erik Olsen

Organizing committee:

Conference chairman: Prof. Stein Tore Johansen
Conference coordinator: Dr. Jan Erik Olsen
Dr. Bernhard Müller
Dr.Sigrid Karstad Dahl
Dr.Shahriar Amini
Dr.Ernst Meese
Dr.Josip Zoric
Dr.Jannike Solsvik
Dr.Peter Witt

Scientific committee:

Stein Tore Johansen, SINTEF/NTNU
Bernhard Müller, NTNU
Phil Schwarz, CSIRO
Akio Tomiyama, Kobe University
Hans Kuipers, Eindhoven University of Technology
Jinghai Li, Chinese Academy of Science
Markus Braun, Ansys
Simon Lo, CD-adapco
Patrick Segers, Universiteit Gent
Jiyuan Tu, RMIT
Jos Derksen, University of Aberdeen
Dmitry Eskin, Schlumberger-Doll Research
Pär Jönsson, KTH
Stefan Pirker, Johannes Kepler University
Josip Zoric, SINTEF

CONTENTS

A COMPUTATIONAL FRAMEWORK INVOLVING CFD AND DATA MINING TOOLS FOR ANALYZING DISEASE IN CAROTID ARTERY BIFURCATION

Mandar TABIB[1*], **Adil RASHEED**[1†], **Eivind FONN**[1‡]
[1]SINTEF Digital, Trondheim, NORWAY

[*] E-mail: mandar.tabib@sintef.no
[†] E-mail: adil.rasheed@sintef.no
[‡] E-mail: eivind.fonn@sintef.no

ABSTRACT

Cardiovascular diseases, like Carotid Artery Disease and Coronary Artery Disease (CAD) are associated with the narrowing of artery due to build-up of fatty substances and cholesterol deposits (called plaque). Carotid Artery Disease increases the chances of brain stroke. Hence, the main objective of this work is to apply computational tools to help differentiate between the healthy and unhealthy artery (with 25% stenosis) using a combination of Computational Fluid Dynamics (CFD) and data mining tools. In this work, first, the CFD has been qualitatively shown to provide similar results as the experimental Phase-Contrast Magnetic Resonance Imaging (PCMRI) technique. The CFD simulation shows that wall shear stress is an ideal parameter to identify the location of plaque formation and the existence of plaque conditions in the body (due to overall higher spatially averaged wall shear stress in the clogged case at all times in the cycle). Then data mining tools like Fast Fourier Transform (FFT) and Proper Orthogonal Decomposition (POD) have been used to unearth a pattern that can be useful for diagnosis. FFT shows that the flow constriction induced by plaque leads to lesser variation in magnitudes of energy of dominant frequencies at different locations like, wake region, mid-Internal Carotid Artery (mid-ICA) and mid-Common Carotid Artery (mid-CCA) regions, while for cleaner artery, there is more variation in the magnitude of energy of these dominant frequencies when measured at wake, mid ICA and mid CCA region. POD helps by confirming the location of regions with high energy in decomposed velocity modes for both the cases. More studies are required to develop a data mining based modern 21st century cardio-vascular patient care.

Keywords: Carotid Artery Bifurcation, CFD , Cardiovascular, data mining. .

NOMENCLATURE

Greek Symbols

ρ	Mass density, $[kg/m^3]$
ϕ	Orthogonal modes, []
λ	Eigen values, []

Latin Symbols

a	POD Coefficients, [].
p	Pressure, $[Pa]$.
$\mathbf{u}$	Velocity, $[m/s]$.
$\mathbf{A}$	Eigen vectors, $[m/s]$.

Sub/superscripts

i	Index i.
j	Index j.

INTRODUCTION AND OBJECTIVE

Cardiovascular diseases, like Carotid Artery Disease and Coronary Artery Disease (CAD), both have some similarities. The similarities in disease progression pertains to the narrowing or hardening of the artery due to build-up of fatty substances and cholesterol deposits (called plaque). Carotid Artery Disease refers to this disease in the artery located in the neck region, and it increases the chances of ischemic strokes and transient ischemic attacks (brain stroke for example). For treatment of such diseases, an in-vivo assessment of physiologic hemodynamics can prove to be beneficial as it might help in understanding the physics behind the development of the vascular diseases. Such investigations may play an important role in designing novel and efficient treatment plans, like Magnetic Drug Targeting (MDT), wherein the magnetized drug particles are added to the blood in the artery and they are made to concentrate around the diseased region by applying a magnetic field at that location. This minimizes the side effects in the rest of the body. However, for such drug delivery methods, it is necessary to accurately determine the flow profiles in the Carotid Artery and to understand the progression of disease. Current methods of evaluating progression of vascular diseases (stenosis, atherosclerosis and aneurysms) involve:a) Experimental techniques (like Phase-Contrast Magnetic Resonance Imaging (PCMRI) (Barker *et al.*, 2010; Markl *et al.*, 2003; Cebral *et al.*, 2009), doppler ultrasound (US), etc) that provide information on the temporal evolution of the velocity profiles, and b) Computational Fluid Dynamic (CFD) techniques (Cebral *et al.*, 2009; Rispoli *et al.*, 2012) where patient-specific angiogram acquired by either Magnetic Resonance Angiography (MRA), or Computed Tomography Angiography (CTA) or 3D Rotational Angiography (3DRA) provide required geometry and flow or pressure waveforms obtained from phase-contrast MRI (PCMRI) as boundary conditions to numerically solve blood flow motion equations in the region of interest and predict hemodynamic parameters over the whole 3D computational domain. Both CFD and experimental techniques have proven to be immensely useful despite the known limitations with both of them (like in experimental techniques, there is low spatial and temporal resolution of PCMRI which limits detection of high velocity gra-

dients, secondary flows and complex flows in recirculation zones, while in CFD - there is the issue of realistic velocity profiles and rigid wall boundary). This success, despite the limitations, can be further enhanced by introducing the ability to unearth more information (and patterns) in order to enable diagnosis from the CFD and experimental dataset. This can be done through application of data mining tools. Researchers involved in evidence-based cardiological practice have suggested that data mining can be the 21st century approach towards patient care (Hu *et al.*, 2009). Data mining (DM) techniques can make cumbersome CFD / Experimental analyses more productive for future everyday clinical practice. Hence, this work focusses on developing a computational framework involving a combination of CFD and data mining techniques like Proper Orthogonal Decomposition (POD) and Fast Fourier Transform (FFT) with the aim of making data mining the workhorse in carotid artery examination and stenosis classification. POD has been widely used to extract dominant modes and structures from massive dynamic computational data to improve the understanding and discovery of the phenomena. The objective of the current work is then to:

Objectives

Develop and demonstrate a computational framework involving CFD and data mining tools (involving feature extraction through POD and FFT) for efficient diagnosis of carotid artery disease progression.

APPROACH AND METHODS

The approach involves investigating two cases: one with carotid artery bifurcation for a healthy person and another for a patient with about 25 % stenosis (meaning that about 25% of the area has been blocked by the plaque formation). First, results from simulations are validated using existing experimental PCMRI data for a similar geometry for a healthy person. In the following step deviations in the flow patterns and wall shear stress for healthy and patient case is demonstrated. Then, the simulated result data is subjected to FFT and POD analysis to obtain more information, and extract the differences. The next section describes the numerical methods (CFD and POD) that are used in the analysis.

CFD

A transient 3D Navier Stokes equation have been solved to simulate the laminar flow in the artery. The model computes the flow fields (velocity, pressure). The Navier−Stokes equations are represented by the mass continuity equation (equation 1) and the momentum transport equation (Equation 2).

$$\nabla \cdot (\rho \mathbf{u}) = 0 \tag{1}$$

$$\frac{D\mathbf{u}}{Dt} = -\nabla \left(\frac{p}{\rho}\right) + \frac{1}{\rho}\nabla \cdot \mathbf{R} \tag{2}$$

where, where ρ is the density, u refers to flow velocity, operator $\frac{D}{Dt}$ refers to total derivative, ∇ refers to gradient-vector operator, $\nabla\cdot$ refers to a partial derivative operator that computes dot product, p is pressure, t is time. $\mathbf{R}$ is referred to stresses arising due to viscosity. Components of $\mathbf{R}$ can be computed as $R_{ij} = \nu\left(\frac{\partial u_i}{\partial x_j} + \frac{\partial u_j}{\partial x_i}\right) - \frac{2}{3}k\delta_{ij}$, where subscripts i, j refers to components of vector, k is turbulent kinetic energy and ν is molecular diffusivity.

Proper Orthogonal Decomposition (POD)

For the computation of the POD modes two dimensional snapshots of any variable (velocity components here) is required. The N snapshots are represented by $\mathbf{U} = [\mathbf{u^1}, \mathbf{u^2} \cdots \mathbf{u^N}]$ which is used to compute the covariance matrix given by $\mathbf{C} = \mathbf{U^T U}$. After this an eigenvalue problem $\mathbf{C A}^i = \lambda_i \mathbf{A}^i$ is solved to obtain the eigenvalues λ^i and eigen vectors $\mathbf{A}^i$ which are sorted in a decreasing order as $\lambda_1 > \lambda_2 > \cdots > \lambda_N$. POD modes are then computed as

$$\phi^i = \frac{\sum_{n=1}^{N} A_n^i \mathbf{u}^n}{||\sum_{n=1}^{N} A_n^i \mathbf{u}^n||}, i = 1, \cdots, N \tag{3}$$

With POD modes arranged as $\Psi = [\phi^1 \phi^2 \cdots \phi^N]$. POD coefficients a_i can be found from the snapshot n as $\mathbf{a}^n = \Psi^T \mathbf{u}^n$. From this a snapshot can be reconstructed as $\mathbf{u}^n = \Psi \mathbf{a}^n$. Relative energy given by any i^{th} mode is given by $\lambda_i / \sum_{j=1}^{N} \lambda_j$

MODEL DESCRIPTION

Figure 1 shows the geometry of the clean healthy artery and an unhealthy clogged artery. In both the cases, the structure involves the main artery (CCA) which bifurcates into the Internal Carotid Artery (ICA) and the External Carotid Artery (ECA).In case of clogged artery, 25% of the flow area in Carotid sinus region has been blocked by plaque deposits. Figure 2 shows the hexahedral mesh that is used to spatially discretize the geometry and the boundary conditions are also labeled. The mesh size is about 3 million element mesh. The mesh resolution is such that across the inlet diameter there are 20 mesh points, resulting in a grid size of 2.5 x $10^{-4}m$ with the grid becoming much finer near the artery surface (about 3x$10^{-5}m$) to capture the high velocity gradients here. The inlet profile used for the study is shown in Figure 3. This inlet velocity profile is based on a heart rate of 72 beats per minute (resulting in 0.8 s time period for one cycle or one beat) which involves the diastolic period for first 0.36 s of cycle (where sinusoidal pulsatile inflow varies with 1.25 Hz frequency (f)) and a systolic period for rest of cycle where inlet velocity is held constant at 0.15 m/s. As a result of this, the normal Peak systolic Velocity (PSV) in the CCA reaches about 0.8 m/s, however in general, the PSV is patient or person specific and depends upon cardiac output or stroke volume, heart rate, systolic blood pressure, and age. The PSV in the normal CCA ranges from 0.70 to 1 m/s while the diastolic velocity is around 0.1-0.2 m/s. Thus, the current inlet profile used is justifiable. The equation used for inlet profile is as proposed by Sinott (Sinnott *et al.*, 2006). The simulations have been conducted over a time period of 12 cycles and the averaging of results has been done over last 2 cycles. An adaptive time-step has been used to maintain a courant number of 1 for accurate and stable simulation, as a result the simulation time step varied between 2.5 x $10^{-5}s$ to 1 x $10^{-4}s$ during the course of simulation. The CFD takes about 1.5 hrs of computational time to simulate one cardiac cycle (time period of one cardiac cycle is 0.8 s) on 8 processors run (with each processor having 1.2GHz CPU speed). For 12 cardiac cycles, about 18 hrs of computational time is required. In the model (Figure 2), the blood flows through the bifurcating artery from the inlet and exits from the two outlets. The density of blood is 1060 kg/m^3. The diameter of the artery at the inlet is around 6 mm. The diameter of ICA outlet is around 4.5mm and the diameter of ECA outlet is around 3.0mm. The Reynolds number based on input diameter varies from around 50 to 300 during the cycle and the flow is considered laminar. The systolic pressure of a healthy

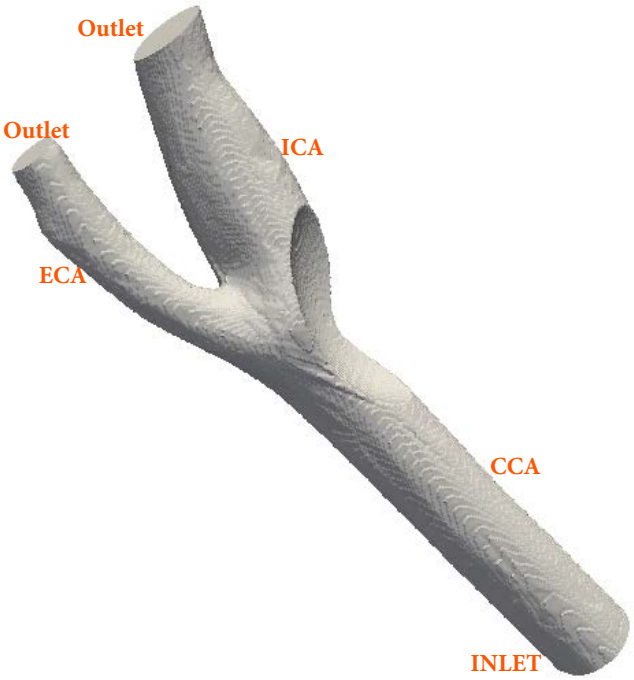

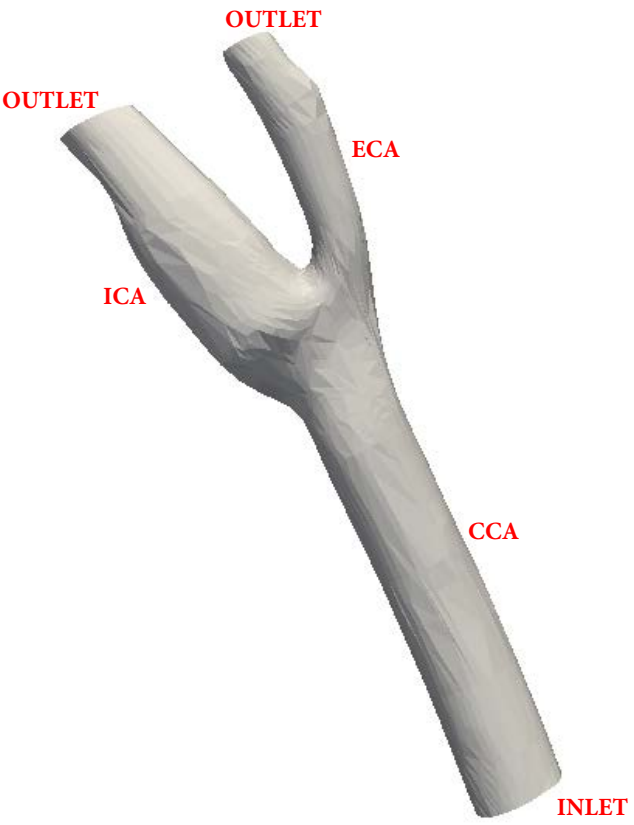

(b) Clean Artery

Figure 1: 3D Geometry of Carotid Artery for clogged and clean case.

(a) Clogged Artery

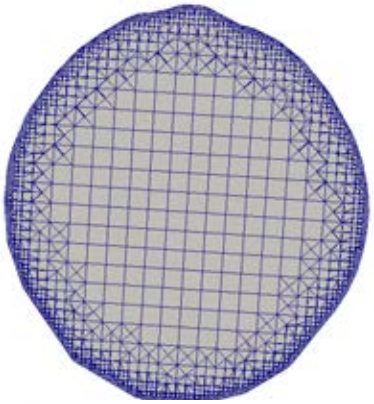

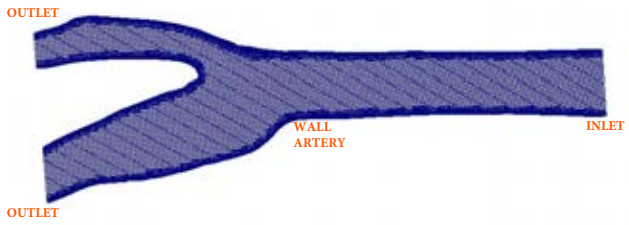

(c) Clean Artery

Figure 2: Mesh and boundary details for clogged and clean case.

human is around 120 mmHg and the diastolic pressure of a healthy human is around 80 mmHg. Thus taking the average pressure of the two phases, we use 100 mmHg (around 13332 Pascal) as the static gauge pressure at the outlets. In the next section, the results obtained from the CFD and data mining tools are discussed.

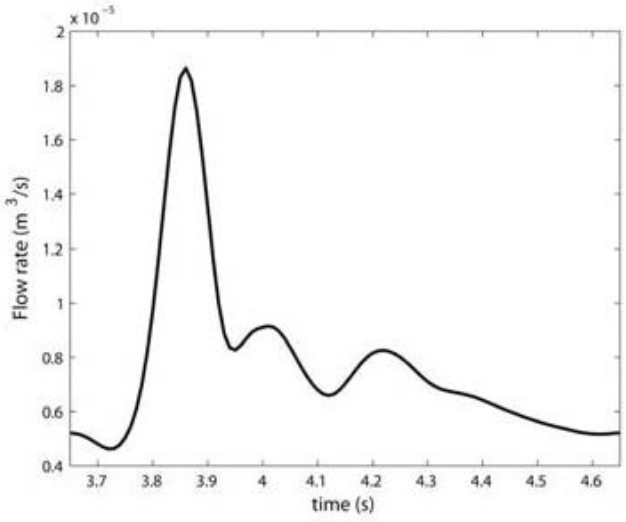

(a) Experimental Inlet Profile is taken from (Gharahi *et al.*, 2016)

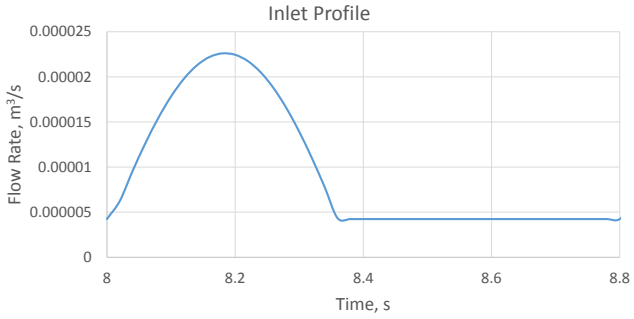

(b) Idealized CFD Inlet

Figure 3: Inlet profiles of experimental and CFD study used in validation.

RESULTS

Validation

Figure 4 involves a quantitative and qualitative comparison study with experimental data obtained from (Gharahi *et al.*, 2016). An attempt is made to check whether CFD is able to predict similar flow patterns in the post bifurcation regions: Internal Carotid Artery (ICA) and External Carotid Artery (ECA) as the experimental data if they begin with similar velocity magnitude in the main artery region. The maximum value of velocity in the contour plot in Figure 4 measured by PCMRI for CCA section is 0.7 m/s, and for the ECA/ICA section is 0.5 m/s. The comparison is done at a time instant corresponding to peak systolic inlet velocity. The velocity from CFD simulations is normalized to match those of the inlet conditions of the experimental data, though some variations in the inflow profile exist as inflow profile in the CFD simulation is an idealized form of the experimental conditions (see figure 3). Qualitatively, CFD is able to predict similar flow patterns as captured by MRI, but quantitatively CFD is over-predicting the magnitude. The deviation ($U_{experimental} - U_{simulation}$)/$U_{experimental}$ in predicting the maximum velocity is around 15% . The difference can be attributed to either low resolution of the MRI data (as seen in figure 4) or variations in the inflow conditions at CCA (again see figure 3). The inflow conditions are shown over one cardiac cycle and it is periodic over this time period. However, the qualitative similarities between the experimental and CFD approach establishes credibility of the CFD study to a certain degree. The major drawback of experimental technique like PCMRI is that owing to its low resolution, it is difficult to compute the wall shear stress, which is known to play a big role in facilitating plaque deposition. Hence, CFD is used to compare the flow field and wall shear stress profiles.

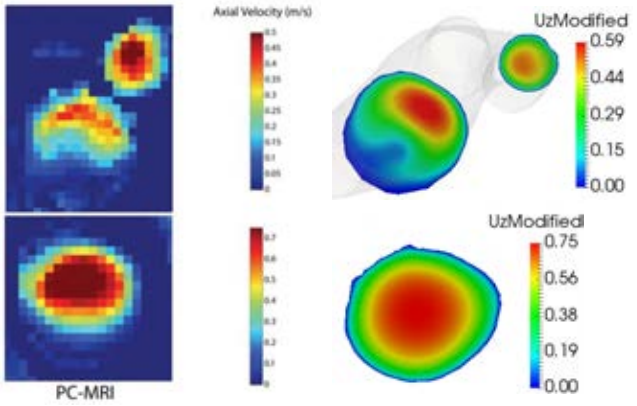

Figure 4: Comparison CFD with PC-MRI Flow pattern. Experimental results in figure on left from (Gharahi *et al.*, 2016)

Comparison of flow patterns

Figure 5 compares the flow patterns for a healthy clean artery and an unhealthy clogged artery for similar inflow conditions. The flow patterns are compared at two instances in each case: at the maximum inlet velocity condition (Figure 5(a) and 5(c)) and at the minimum inlet velocity condition (figure 5(b) and 5(d)). In the clogged case (figure 5(c)-5(d)), the streamlines show higher flow separations and flow recirculations than the clear artery case (figure 5(a)-5(b)) near the carotid bulb both at the minimum velocity and maximum velocity inlet conditions. The resulting helical and secondary flows (due to flow separations around complex artery geometry) are higher at maximum inlet velocity conditions than the minimum velocity conditions. The impact of these flow patterns is felt on the wall shear stress as well as the associated frequencies (the FFT's are conducted at the probe locations denoted by black dots between the text P1, P2 and P3 in figure 5 and discussed in the section on FFT comparison.

Comparison of wall shear stress

Figure 6 and 7 compare the wall shear stresses for the two conditions. Figure 6 presents the wall stress at two instances for both healthy and unhealthy case one at the maximum inlet velocity condition and another at the minimum inlet velocity condition. In the clogged case (Figure 7(c)-7(d)), a higher wall shear stress compared to the clear artery case (figure 7(a)-7(b)) is seen. This can be attributed to the higher velocity gradients owing to the blockage of the flow area and higher flow recirculations behind the plaque deposits. The location of the plaque is at the ICA region, where sudden divergence cause recirculation with low velocity gradient region causing regions of lower shear stress. In both the cases,

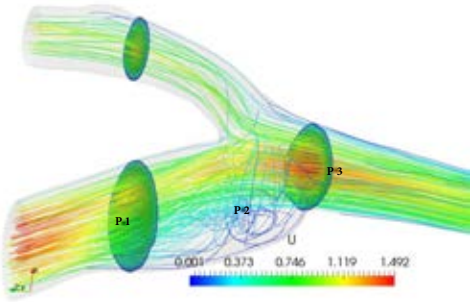

(a) Clean Artery at Max U_{inlet}

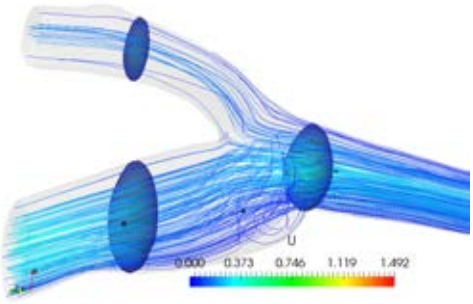

(b) Clean Artery at Minimum U_{inlet}

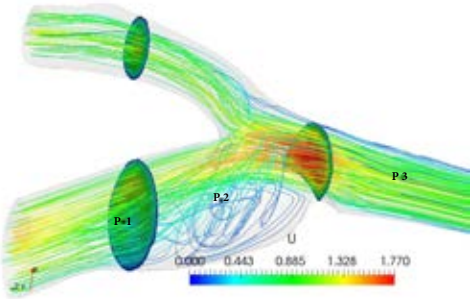

(c) Blocked Artery at Max U_{inlet}

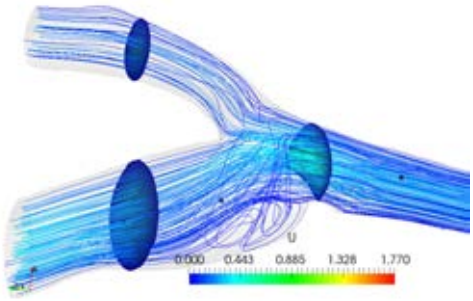

(d) Blocked Artery at Minimum U_{inlet}

Figure 5: Flow pattern and streamlines comparison for clogged and clean artery.

the wall shear stress has the highest magnitude near the inner wall of the carotid bifurcation and conversely, the ICA displays lower wall shear stress.

Figure 7 compares the spatially averaged wall shear stress over the whole artery over two period of cycles. Here too, it can be seen that wall shear stress values are consistently higher for the clogged case over the whole cycle. Thus, the simulation shows that wall shear stress is an ideal parameter to confirm both the location of plaque formation (low wall shear stress region) and the existence of plaque conditions in the body (overall higher spatially averaged wall shear stress in clogged case at all times in the cycle). Next we look at feature extraction from the accumulated dataset to help in the diagnosis of Carotid Artery Disease. FFT and POD have been used in this work.

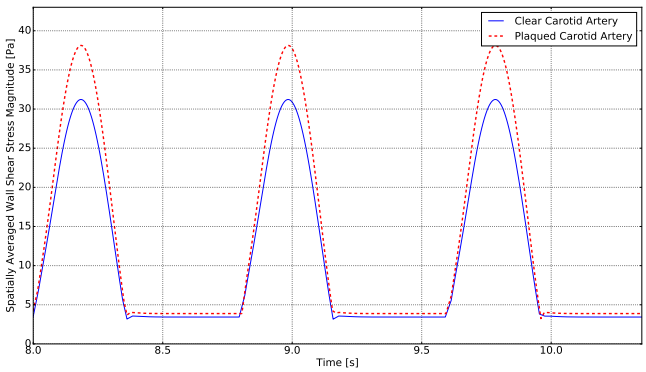

Figure 6: Comparison of wall shear stress at different times in a cycle for clogged and clean artery case.

FFT Comparison

Figure compares the energy spectrum obtained from the application of FFT on the velocity signal at the probe locations for both the clean and clogged artery cases. FFT provides the energies associated with various frequencies and helps to identify the dominant frequencies. The location of probes is shown as black dot in Figure 5. FFT is compared at probes located in the CCA, ECA and wake regions. The data is sampled at a frequency of 10000 Hz over a period of 2 cycles. All the probe locations in both the cases are able to detect the dominant frequency of 1.25 Hz present in the inlet pulsatile flow at varying magnitudes. The bifurcation region which creates a diverging section at the ICA leads to the presence of eddies in flow separation, with these eddy having its own length and time-scale. For the clean artery case , figure 8(a) shows that the energy of dominant frequency (1.25 Hz) in the wake region is less than that at the CCA and ICA case but a high amount of fluctuations in frequency range 10-20 Hz range is seen. These fluctuations could be representative of eddies arising out of flow separation and some of them possess similar energy content as the dominant frequency in the wake region (energy range above $1x10^{-}3m^2/s^2$). While in the wake region of clogged artery case, figure 8(b) shows the energy in dominant frequency (1.25Hz) and energy in fluctuations in 10-20 Hz in to be more nearer to the energy in corresponding frequencies in the ICA and CCA region (as compared to the clean artery case). The blockage induced by plaque leads to higher velocity magnitudes and higher flow recirculation leading to higher energy frequencies (at both 1.25Hz and 10-20 Hz range) and leading them to be closer to energies associated with these frequencies in ICA and CCA

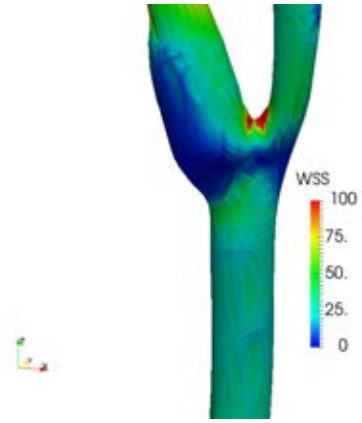

(a) Clean Artery at Max U_{inlet}

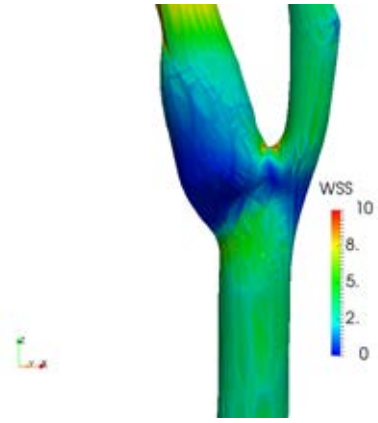

(b) Clean Artery at Minimum U_{inlet}

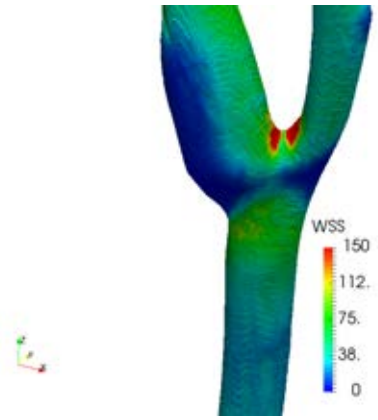

(c) Blocked Artery at Max U_{inlet}

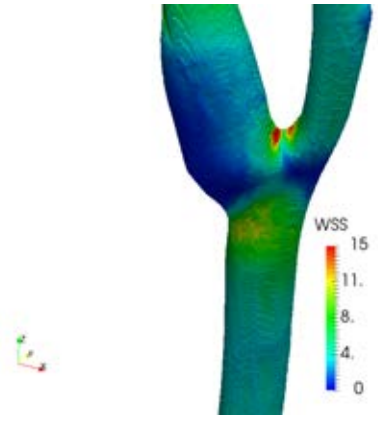

(d) Blocked Artery at Minimum U_{inlet}

Figure 7: Wall Shear Stress contour comparison for clogged and clean artery case.

(as compared to clear artery case). Such patterns as this, which has been identified by FFT can be an useful detection and diagnosis tool. Though more studies are required to ascertain presence of such patterns. The location of regions of higher energies can be obtained from the POD analysis as shown below.

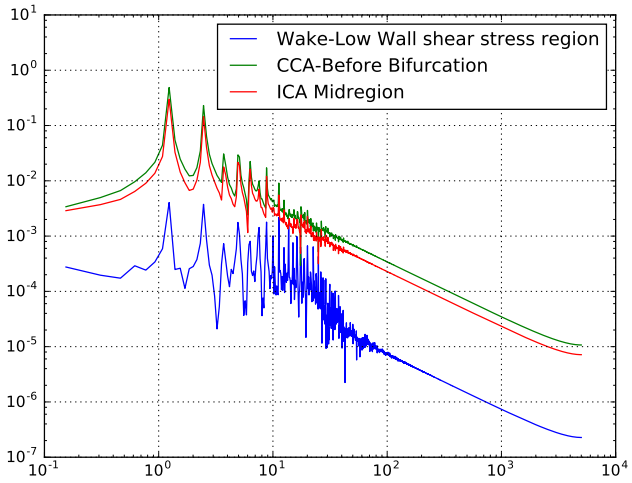

(a) Clean Artery, X axis is Frequency in Hz, and Y axis is Energy in m^2/s^2

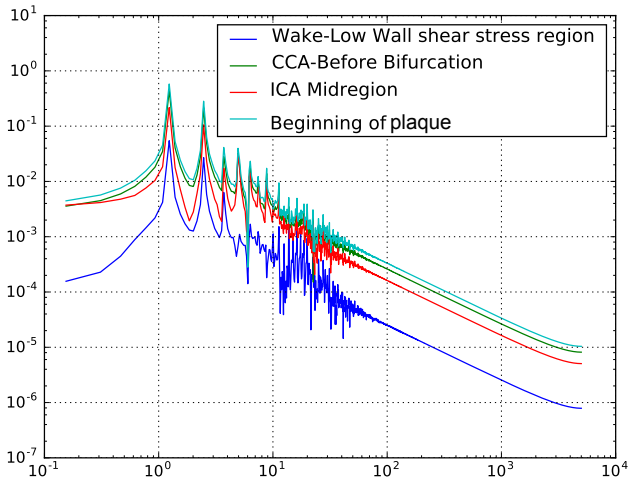

(b) Clogged Artery, X axis Frequency in Hz, and Y axis is Energy in m^2/s^2

Figure 8: FFT results for clogged and clean artery case.

POD comparison

For Artery, the 2D planar data for each simulation is sampled at 5 Hz and then interpolated on a uniform rectilinear grid measuring 510×159 elements (corresponding to a grid-size of $0.0509mm \times 0.0158mm$). The original snapshots (defined on the original mesh) have been interpolated on a uniform mesh (defined on a rectangle), so the modes are also defined on the whole rectangle, even though they are zero outside of the artery region. The results regarding the energy spectra can be observed in Figure 9, which reveals that there is not much difference in energy captured by different modes. In both the cases, almost more than 99% of energy is captured within the first two modes itself, the first mode being the large scale flow and second mode being mostly the separated flow in the wake region (as seen in figure 10- 11 which shows the decomposed velocity modes for the two cases). Despite similar energy content of the modes in the two cases, the location of concentration of energy is different. Figures (10-

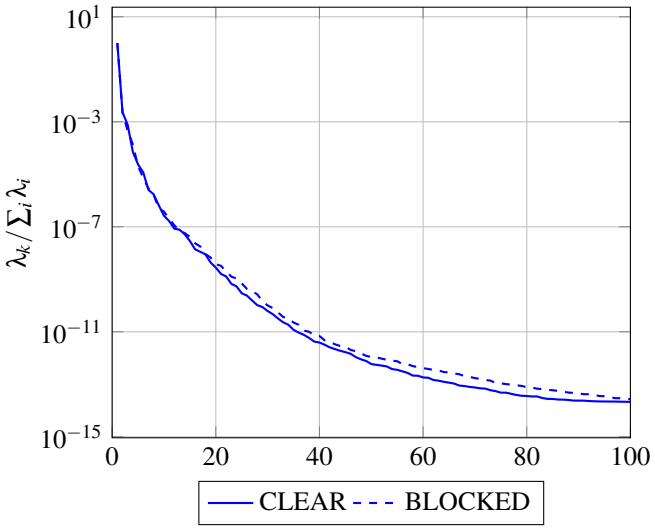

Figure 9: ENERGY SPECTRA OF CLEAR AND BLOCKED ARTERY.

11) show the decomposed velocity modes, where the Red color regions represent regions with highest decomposed velocity values and blue color regions represents regions with lowest decomposed velocity values. The values of these decomposed modes are not relevant. These figures (figure 10-11) reveal that mode 1 has similar energy of around 99.7% for both case, but in case of clogged artery, most of this energy is concentrated in the region above the plaque where the flow constriction leads to higher by the plaque. Similarly, de-

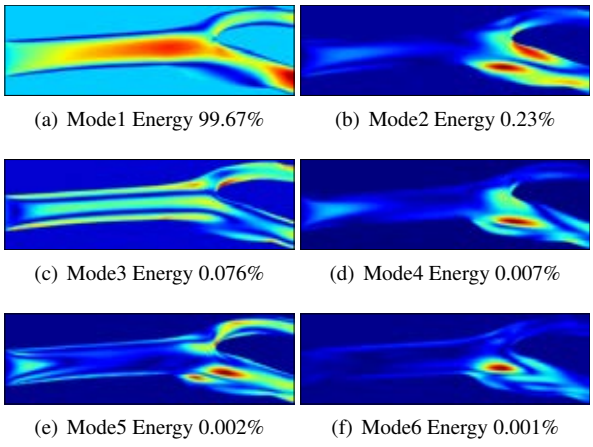

(a) Mode1 Energy 99.67% (b) Mode2 Energy 0.23%

(c) Mode3 Energy 0.076% (d) Mode4 Energy 0.007%

(e) Mode5 Energy 0.002% (f) Mode6 Energy 0.001%

Figure 10: First six modes of a healthy artery showing decomposed velocity. Red color regions represent regions with highest decomposed velocity values and blue color regions represents regions with lowest decomposed velocity values.

spite mode 2 capturing the energy content of around 0.22%, the clogged one has energy concentrated around wake region while the clean artery case has this energy distributed in both wake at outer wall of ICA and energy at the inner wall of the ICA. This energy distribution also shows the reasoning behind the pattern observed through FFT analysis.
Thus, the POD and FFT together as data mining tools helped to unearth the differences between healthy and unhealthy patients artery. These tools can be applied on experimental dataset as well if there is a possibility to obtain suitable variable dataset at the required locations at high sampling rate. CFD provides a cost effective way of obtaining data at high sampling rates and at all locations in the geometry (which is sometimes difficult to do using experiments).

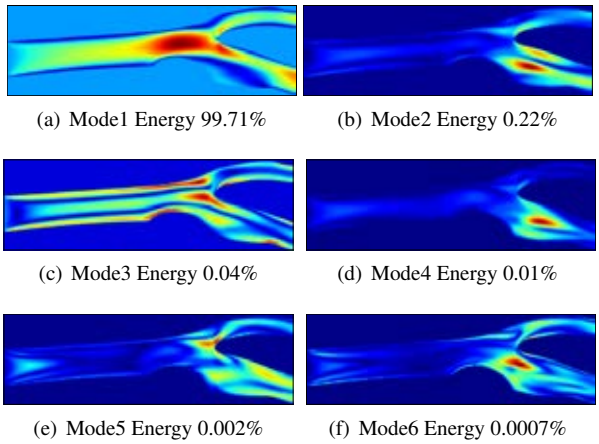

(a) Mode1 Energy 99.71% (b) Mode2 Energy 0.22%

(c) Mode3 Energy 0.04% (d) Mode4 Energy 0.01%

(e) Mode5 Energy 0.002% (f) Mode6 Energy 0.0007%

Figure 11: First six modes of an unhealthy clogged artery showing decomposed velocity. Red color regions represent regions with highest decomposed velocity values and blue color regions represents regions with lowest decomposed velocity values.

CONCLUSION

The work demonstrates an application of combination of CFD along with data mining techniques in unearthing differences between a healthy and an unhealthy patient with carotid artery disease. The conclusions are enumerated below :

1. First, the CFD has been qualitatively shown to provide similar results as the experimental PCMRI technique. Owing to lower resolution of the experimental technique, CFD has been used to analyze further differences in the flow pattern.

2. CFD simulation shows that wall shear stress is an ideal parameter to show existence of plaque conditions in case of unhealthy artery (overall higher spatially averaged wall shear stress in clogged case at all times in the cycle).Further CFD shows the observation of lower wall shear stress in regions of carotid sinus where build up of plaque occurs.

3. Use of data mining tools (FFT and POD) along with CFD has helped to unearth patterns to distinguish between healthy and unhealthy case. FFT shows that the flow constriction induced by plaque leads to lesser variation in magnitudes of energy of dominant frequencies at different locations (like, wake region, mid-ICA and mid-CCA region), while for cleaner artery, there is more variation in magnitude of energy of these dominant frequencies when measured at wake, mid ICA and mid CCA region. POD helps by confirming the location of regions with high energy in decomposed velocity modes for both cases. Such patterns as this, which has been identified by FFT can be an useful detection and diagnosis tool.

This work is one of the steps towards using data mining for modern 21st century cardiovascular patient care. Future

work involves using this methodology for more studies involving different patients and healthy persons to confirm the observed patterns and develop a diagnosis toolkit.

REFERENCES

BARKER, A., BOCK, J., LORENZ, R. and MARKL, M. (2010). "4d flow mr imaging". *Am J Neuroradiol.*, **18**, 46.

CEBRAL, J., PUTMAN, M., ALLEY, M., HOPE, T., BAMMER, R. and CALAMANTE, F. (2009). "Hemodynamics in normal cerebral arteries: Qualitative comparison of 4d phase-contrast magnetic resonance and image-based computational fluid dynamics." .*J Eng Math.*, **64**, 367.

GHARAHI, H., ZAMBRANO, B., ZHU, D., DEMARCO, J. and BAEK, S. (2016). "Computational fluid dynamic simulation of human carotid artery bifurcation based on anatomy and volumetric blood flow rate measured with magnetic resonance imaging". *Int J Adv Eng Sci Appl Math.*, **8**, 40.

HU, D., NGUYEN, T., KIM, M., KWAN, T. and SAITO, S. (2009). "Evidence-based cardiology practice: A 21st century approach". *PMPH*, **1**, ISBN: 978–1–60795–095–0.

MARKL, M., CHAN, F., ALLEY, M., WEDDING, K., DRANEY, M. and ELKINS, C. (2003). "Time-resolved three-dimensional phase-contrast mri". *J Magn Reson Imaging*, **17**, 499.

RISPOLI, V., CARVALHO, L., NIELSEN, J. and NAYAK, K. (2012). "Assessment of carotid flow using magnetic resonance imaging and computational fluid dynamics". *Fluid dynamics, computational modeling and applications. Editor Juarez LH. InTech*, **64**, 513.

SINNOTT, M., CLEARY, P. and PRAKASH, M. (2006). "An investigation of pulsatile blood flow in a bifurcating artery using a grid-free method". *Fifth International Conference on CFD in the Process Industries CSIRO, Melbourne, Australia*.